Nuclear Instruments and Methods in Physics Research A 728 (2013) 133–144

Contents lists available at SciVerse ScienceDirect

Nuclear Instruments and Methods in Physics Research A

journal homepage: www.elsevier.com/locate/nima

Technical Notes

Uncertainty minimization in NMR measurements of dynamic nuclear polarization of a proton target for nuclear physics experiments

D. Keller *

University of Virginia, Charlottesville, VA 22901, United States

ARTICLE INFO

Article history:
Received 19 February 2013
Received in revised form
12 June 2013
Accepted 27 June 2013
Available online 4 July 2013

Keywords:
Uncertainty minimization
NMR
Dynamic nuclear polarization
Proton target

ABSTRACT

A comprehensive investigation into the measurement uncertainty in polarization produced by Dynamic Nuclear Polarization is outlined. The polarization data taken during Jefferson Lab experiment E08-007 is used to obtain error estimates and to develop an algorithm to minimize uncertainty of the measurement of polarization in irradiated $^{14}NH_3$ targets, which is readily applied to other materials. The target polarization and corresponding uncertainties for E08-007 are reported. The resulting relative uncertainty found in the target polarization is determined to be less than or equal to 3.9%.

1. Introduction

Nuclear and particle physics experiments using solid polarized targets attempt to extract a number of polarized observables, frequently an asymmetry associated with the target polarization. As a result, a large contribution to the observables systematic uncertainty can come from the limited precision in the Nuclear Magnetic Resonance (NMR) measurement of polarization.

The uncertainty in the calibration of the polarization measurement primarily comes from measurement limitation of area of the NMR signal and temperature of the target material at thermal equilibrium. There is also an uncertainty in the polarization caused by changes in the experimental environment that can affect the NMR signal or the coupling of the target material to the NMR circuit. In order to accurately represent and minimize the experimental error, it is important to determine when such changes have and have not occurred.

There are several contributions to polarization uncertainty that depend on the experimental configuration such as target length, beam intensity, and target material type. For the error analysis presented here the focus is on proton targets using $^{14}NH_3$ at the electron beam intensity of (~100 nA) which is of most interest for past and future Thomas Jefferson National Accelerator Facility (TJNAF) Hall A and Hall C polarized target experiments. There have already been multiple experiments with similar beam intensity such as E93-026, E01-006, E08-027, E07-003, and E06-014 at Jefferson Lab and E143, E155, and E155x at SLAC. High intensity beams lead to quicker polarization decay and can also lead to more frequent changes in the materials ability to polarize and hold polarization. The effects on systematics from these changes can be taken into account with frequent NMR target calibration measurements and careful control of the beam size on the target face.

During an experiment, the number of target calibration measurements may be limited due to time constraints resulting in a larger uncertainty in the target data that is not well defined. Here a systematic procedure is outlined to obtain the integrated systematic uncertainty associated with a single calibration measurement over a section of physics data. A minimization can then occur with multiple target calibrations on consecutively used material. A χ^2-minimization technique is used weighting each calibration by its combined total uncertainty. To illustrate these details a full target data analysis for TJNAF Hall A experiment E08-007 is completed obtaining the final polarization for each production run and the associated polarization uncertainties. Though a proton target is used the procedure presented is readily applied to any polarized target material which uses a thermal equilibrium calibrated NMR to probe polarization during nuclear physics experiments.

The goal of experiment E08-007 was to study the proton elastic form factor ratio $\mu G_E/G_M$ in the range $Q^2 = 0.01–0.7\ \mathrm{GeV}^2$. The experiment was carried out with the hope of improving the knowledge of the ratio at low Q^2. In this low Q^2 range, substantial deviations of the ratio from unity have been observed [1–3], and

* Tel.: +1 434 924 6799.
E-mail address: dustin@jlab.org

0168-9002
http://dx.doi.org/10.1016/j.nima.2013.06.103

data, along with many fits and calculations, continues to suggest that structures might be present in the individual form factors, and in the ratio. Experiment E08-007 made precise measurements of the polarized beam–polarized target asymmetry which can be used in an attempt to resolve these possible structures.

The experiment took place using the TJNAF Continuous Electron Beam Accelerator Facility (CEBAF) in Hall A with the beam energy between 1.1–2.2 GeV at a beam current of 100 nA.

2. The solid polarized target

A solid polarized target has the advantage over gaseous targets of being high in nucleon density. In addition the nucleon density can also be made very stable within the temperature control of the cryostat. Combined with high beam current solid polarized targets provide the highest luminosity experiments that can be done to extract polarized target observables.

Dynamic Nuclear Polarization (DNP) of the solid material used in nuclear experiments can be achieved at ~1 K using a homogeneous magnetic holding field and a microwave field to transfer the polarization to the nuclear spins. For materials of interest DNP is not well described by the solid-state effect in which the interaction between paramagnetic spins can be neglected. The equal spin temperature theory is required to address dipolar interactions between electrons seen in materials with high electron density. The spin–spin interaction between electrons produce a separate energy reservoir dependent on the Zeeman and lattice energies only through the characteristics of transverse relaxation and diffusion. The nuclei become polarized by the coupling of the nuclear spin and the paramagnetic spin systems. Microwaves are used to change the spin temperature, which in turn interacts with the proton Zeeman system. Nuclear spin relaxation must be orders of magnitude slower than the relaxation of the paramagnetic centers so that the rate of polarization is higher than the rate of depolarization allowing polarization to be built and maintained by the microwaves. Depending on the tuning of the microwave frequency the proton spins become polarized parallel or antiparallel to the magnetic field. As an example using microwaves of slightly less than the Zeeman energy leads to the spin system emitting energy resulting in transitions that lead to positive spin temperature corresponding to positive polarization. The contrary is true to achieve negative polarization.

For experiment E08-007 the target polarization performance was optimized by the use of irradiated ammonia target material and a high power EIO microwave tube characterized to oscillate in a range around ~140 GHz. The solid polarized target system, see Fig. 1, used a ^{4}He evaporation refrigerator with sufficiently high cooling power to minimize the heating effects of the microwave and high beam current. A 5 T super conducting magnet was used to polarize and maintain polarization of the target during the experiment.

The following includes some introductory discussion on the target material preparation, radiation damage, and performance.

2.1. Preparation of material

Experiment E08-007 required the fabrication of ammonia $^{14}NH_3$ beads to serve as target material. This fabrication was done by the University of Virginia (UVA) polarized target lab [4]. Ammonia gas is condensed by sealing it in a Teflon coated stainless steel tube under a liquid nitrogen (LN_2) bath. This freezes the ammonia into a solid. Once in the solid form, the ammonia is crushed through mesh screens to form beads approximately 2 mm in diameter.

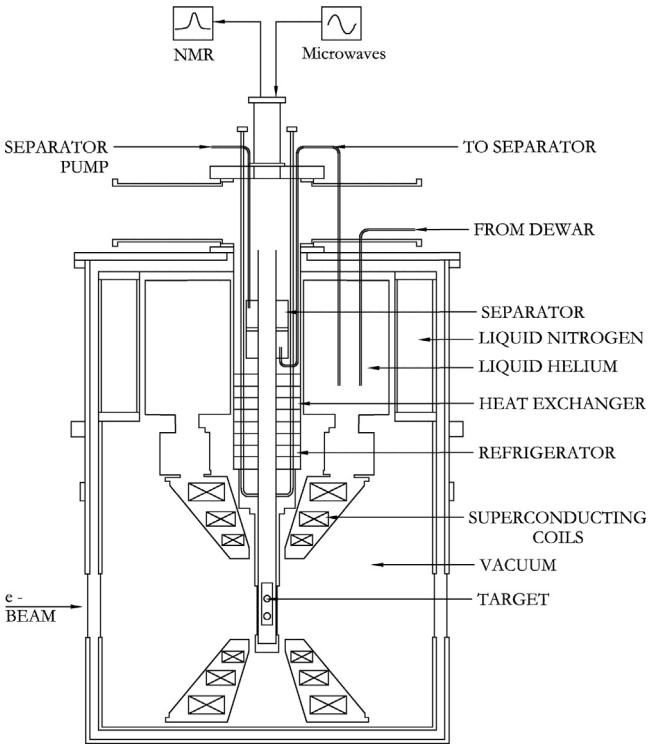

Fig. 1. Polarized target system for NH_3/ND_3 at 5 T used to achieve a temperature of ~1 K.

The ammonia beads for the experiment were then irradiated to introduce paramagnetic radicals to optimize polarization performance [5,6]. The preparation technique used was first developed and implemented with NH_3 in 1979 [7,8]. A high-intensity beam from a traveling-wave electron linac was used to irradiate the ammonia approximately 10^{17} e^-/cm^2 (120 min). The irradiation leads to protons being knocked-out of the NH_3 molecule to form NH_2 paramagnetic centers. The irradiation took place at the Medical Industrial Radiation Facility (MIRF) at the National Institute of Standards and Technology (NIST) in Gaithersburg, MD, using the MIRF 14 MeV electron beam at ~10 μA to strike the material under a ~87 K liquid argon (LA) bath. The prepared material was then stored in liquid nitrogen until installed into the experiment target insert at Jefferson Labs.

2.2. Material radiation damage

Radiation damage to the target material happens when additional radicals in the target materials are created during the experiment. The radiation-produced radicals populate the NH_3 distorting the DNP process. As radical density increases, it affects the relaxation processes, shortening relaxation time and reducing nucleon polarization.

The polarization reduction from radiation damage can be almost completely recovered by heating or annealing the target material, not to exceed about 20 K below the devitrification temperature [9,10]. The amount of radiation damage sustained with the same dose increases after each anneal until the material must be changed. The radiation damage over the course of the experiment can be seen by studying polarization changes with respect to dose on the material from the CEBAF electron beam. The beam dose is measured as electrons pass into the circular area of the target cell. The charge accumulation is obtained using the Hall A beam current monitors (BCMs) [11]. The polarization as a function of dose is shown in Fig. 2. The same ammonia sample

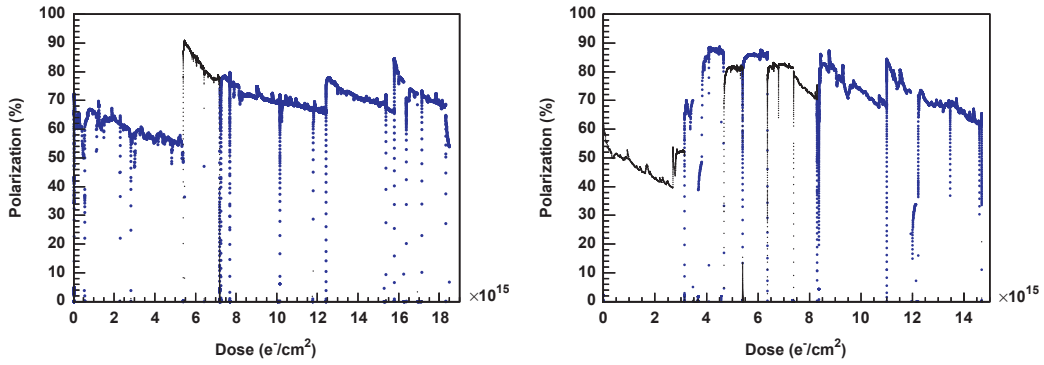

Fig. 2. Polarization with respect to beam dose for the top target cell on the left and the bottom target cell on the right. The large points indicate positively polarized data while the small points indicate negatively polarized data. The solid vertical lines indicate when the anneals took place.

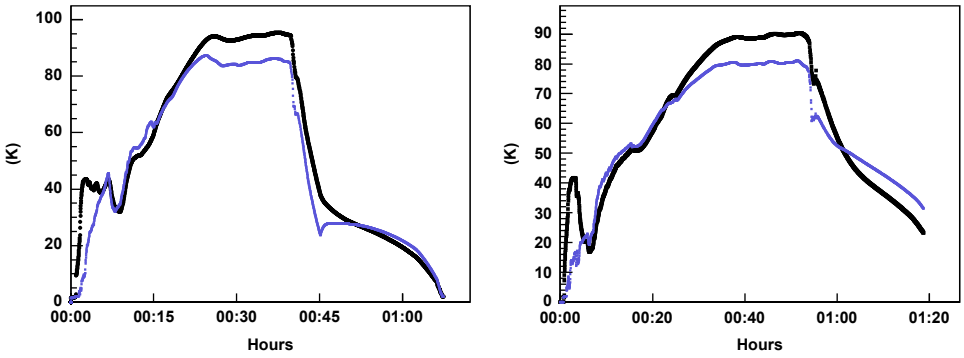

Fig. 3. The temperature and duration for the second anneal (left) and third anneal (right). The temperature of the top target cell is indicated by the thick line and the temperature of the bottom target cell is indicated by the thin line.

in each target cell was used over the entire course of experiment E08-007.

2.3. Material performance and anneals

The material placed in the top target cell was irradiated at NIST for 140 min while the material placed in the bottom cell was irradiated for 120 min. The maximum absolute polarization during the commissioning runs were about 70% for the top cell and 60% for the bottom. The response in polarization of the top cell is an indication of slight over population of paramagnetic radicals present from the NIST irradiation. On the other hand the bottom cell performance tends to increase initially with additional beam dose. After the first anneal, at 5.4×10^{15} e^-/cm^2 (3.1×10^{15} e^-/cm^2) for the top (bottom) cell in Fig. 2, the material performance improved reaching over 90% polarized. The first anneal had an average temperature of about 75 K for 15 min. Over the course of the experiment the anneals require a longer duration at a greater temperature but still less than 100 K. The other two anneals on the target materials are shown in Fig. 3. The solid vertical lines seen in Fig. 2 indicate when the anneals took place.

2.4. Systematic effects of polarization changes

The systematic effect of the reversal of the target polarization is checked by comparing the evolution of the polarization decay in Fig. 2. As seen in the top cell, Fig. 2 (left), the points from positive polarization match with the points from negative polarization in the decay trend. In the bottom cup, Fig. 2 (right), this is less evident because the electron beam was turned on while still attempting to maximize the negative polarization with the microwave. After the cold irradiation of ammonia negative polarization enhancement has a much slower growth than the positive [6]. No uncertainty is added based on positive and negative polarization differences. This serves only as a systematic check.

The electron beam dose history is necessary to charge average polarization over a data run to make the polarized target data available to use in physics analysis. Faster polarization decay due to radiation damage can lead to larger spread in polarization over a data run. This is discussed further in Section 6.

2.5. Homogeneity

High intensity beams have a greater chance of leading to inhomogeneous low temperature irradiation resulting in false polarization sampling of the NMR loop. If the incident electron beam spot size changes or moves inside the target cup over a period of time the NMR will report only an accurate value for the polarization average surrounding the NMR loop. A large polarization differential can develop in the material in just a few hours leading to greater uncertainty in polarization data. When it has been determined that a large polarization differential has developed in the material and the same material is required for additional data collection the best procedure is to remove the material and repack the cup to re-homogenize the material. In general all of these issues are avoided with the careful use of the fast and slow raster beam spreading.

The fast raster system uses two air-core magnets to spread the beam spot from less than 100 μm to 2 mm. Triangle waveforms are used to drive the magnet currents to produce a uniform square beam spot. The slow raster takes the 2 mm square beam and renders a beam spot that nearly fills the target cups of 2.4 cm diameter. Three waveform generators were used to drive the slow raster magnets. The angular velocity of the beam and amplitude modulation was used to uniformly draw the beam through a spiral to form a circular spot.

For experiment E08-007 great care was taken to maintain the beam spot size (2.25 cm) and re-center throughout the various transitions of the experiment. No additional error from material polarization inhomogeneity is added.

3. Polarized target data analysis

The polarized target data is collected during the experiment in a data stream of all NMR and cryogenic control system variables. The polarized target data analysis checks the conditions of the target calibrations, NMR baselines and target data as well as reintegration of the NMR signal to ensure the highest quality of the resulting polarization. Measurement precision of the devices in the NMR system and all other aspects of polarization uncertainty must also be considered. Adjustments to the polarization and total uncertainties are then acquired. The following section discusses the NMR system, the uncertainty in NMR polarization, instrumental contributions from the NMR system devices, and the NMR signal fitting and integration.

3.1. The NMR system

The nuclear spin polarization was measured with a continuous-wave NMR coil and Liverpool Q-meter [12]. The Q-meter works as part of a circuit with phase sensitivity designed to respond to the change of the impedance in the NMR coil. The radiofrequent (RF) susceptibility of the material was inductively coupled to the NMR coil which was part of a series LCR circuit, tuned to the Larmor frequency of the nuclei being probed. The output, consisting of a DC level subtracted by a post Q-meter conditioning card (Yale gain card), was then digitized and recorded as a target event [13].

The polarized target NMR and data acquisition included the software control system, the Rohde & Schwarz RF generator (R&S), the Q-meter enclosure, and the target cavity insert, see Fig. 4. The Q-meter enclosure contained two separate Q-meters and Yale gain cards which were used for different target cup cells during the experiment. The target material and NMR coil are held in polychlorotrifluorethylene (Kel-F) cells with the whole target insert cryogenically cooled to 1 K. Kel-F is used because it contains no free protons.

The R&S generator produced a RF used to drive a triangle wave providing a sweep over the frequency range of interest. The R&S responded to an external modulation sweeping linearly from 400 kHz below to 400 kHz above the Larmor frequency. The signal

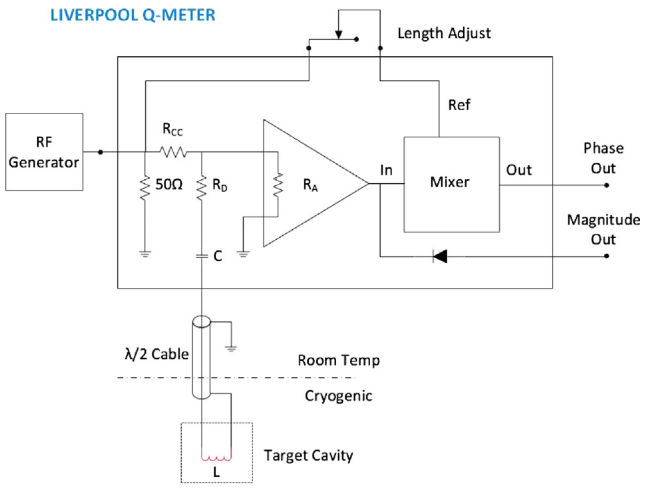

Fig. 4. Schematic diagram depicting the RF generator, the Q-meter, and the target cavity.

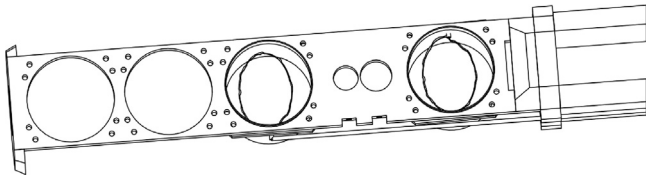

Fig. 5. Drawing of the target insert showing the top (right) and bottom (left) cups with a single loop NMR coil.

from the R&S was connected to the NMR coils within the target material. To avoid degrading reflections in the long connection from the NMR coil to the electronics a standing wave can be created in the transmission cable by selecting a length of cable that is an integer multiple of the half-wavelength of the resonant frequency. This specialized connection cable is known as the $\lambda/2$ cable and is a semi-rigid cable with a Teflon dielectric. The NMR coil contains a single loop made of 70/30 copper–nickel tube, which minimizes interaction with the electron beam. The NMR loop opens up into an oval shape spanning approximately 2 cm inside the 2.4 cm diameter cup. The loop is located about halfway down in the center of the cup. Fig. 5 shows the top and bottom cups with NMR coils. It is possible to enhance signal to noise information through the software control system by making multiple frequency sweeps and averaging the signals. A completion of the set number of sweeps resulted in a single target event with a time stamp. The averaged signal was integrated to obtain a NMR polarization area for that event. Each target event written contained all NMR system parameters and the target environment variables needed to calculate the final polarization. The on-line target data and conditions were analyzed over the experiments set of target events to return a final polarization and associated uncertainty for each run.

3.2. Uncertainty in NMR polarization

A target NMR calibration measurement or Thermal Equilibrium (TE) measurement was used to find a proportionality relation to determine the enhanced polarization under a range of thermal conditions given the area of the "Q-curve" NMR signal at the same magnetic field. The magnetic moment in the external field results in a set of $2J+1$ energy sublevels through Zeeman interaction, where J is the particle spin. The TE natural polarization for a spin-1/2 particle is given by

$$P_{TE} = \tanh\left(\frac{\mu B}{kT}\right) \tag{1}$$

coming from Curie's Law [14], where μ is the magnetic moment in the external field of strength B, k is the Boltzmann constant, and T the temperature. Measuring P_{TE} at low temperature increases stability and the polarization signal. This is favorable being that the uncertainty in the NMR signal increases as the area of the signal decreases. In fact much of the target uncertainty comes from error in the calibration. The goal temperature used is ~1 K.

The dynamic polarization value is derived by comparing the enhanced signal S_E integrated over the driving frequency ω with that of the (TE) signal

$$P_E = G\frac{\int S_E(\omega)\,d\omega}{\int S_{TE}(\omega)\,d\omega}P_{TE} = GC_{TE}A_E \tag{2}$$

and calibration constant defined as

$$C_{TE} = \frac{P_{TE}}{A_{TE}} \tag{3}$$

where P_E (A_E) is the polarization (area) of the enhanced signal and P_{TE} (A_{TE}) is the polarization (area) from the thermal equilibrium

measurement. The uncertainty in the calibration constant, $\delta C_{TE}/C_{TE}$, can easily be calculated using the fractional error from P_{TE} and A_{TE}. The ratio of gains from the Yale card used during the thermal equilibrium measurement to the enhanced signal is represented as G. For experiment E08-007 the same gain setting was used for both but since the input voltage is slightly different at thermal equilibrium than for the enhanced signal, G deviates from unity.

The final uncertainty calculation for $\delta P_E/P_E$ can be expressed as

$$\frac{\delta P_E}{P_E} = \left[\left(\frac{\delta G}{G}\right)^2 + \left(\frac{\delta P_{TE}}{P_{TE}}\right)^2 + \left(\frac{\delta A_{TE}}{A_{TE}}\right)^2 + \left(\frac{\delta A_E}{A_E}\right)^2 + \left(\frac{\delta S_{TE}}{S_{TE}}\right)^2 + \left(\frac{\delta S_E}{S_E}\right)^2\right]^{1/2}. \quad (4)$$

The term δS_{TE} represents the uncertainties acquired during the thermal equilibrium calibration measurements that are based on measurement limitations. The last term δS_E comes from the uncertainty estimates due to the systematic effects over time. These effects can be thought of as variation seen in the enhanced signal over the course of the experiment. The variation in enhanced signal area at fixed polarization and temperature on the time scale of a single experimental run is negligible. For a single experimental run the thermal fluctuations set the upper limit of δS_E which is measured to be smaller than 0.02% in enhanced signal area. However, over the time scale of the experiment fluctuation in the NMR probing system or environmental changes leads to significant contributions to uncertainty.

3.3. Yale card characteristics

The NMR signal from the Q-meter can be amplified by approximately 1, 20 or 50 times using the Yale card gains. There were two complete NMR circuits used in the experimental setup, one for the top target cup and the other for the bottom target cup. Both of the Yale cards were characterized to find a set of gains as a function of input voltage. These results enabled accurate calculation of the final polarization used in data analysis. These gain parameters were determined by sweeping the input voltage over a positive and negative range large enough to determine a clear trend. Fig. 6 shows the trend for the Yale card used for the bottom target cup NMR configuration. The results shown are for the amplification of 1.

The Q-meter output voltage includes a DC offset of ~3 V whereas the change from TE to enhanced signal prior to gain amplification is on the order of ~100 mV. The Yale gain amplifies this processed signal after which the DC offset is subtracted out. The ratio of gains form the Yale card used during the thermal equilibrium measurement to the enhanced signal is obtained by dividing the gain from an averaged enhanced signal input voltage by the gain from an averaged TE signal input voltage leading to $G=0.999213$. This gain is used in the polarization calculation in Eq. (2). Because the gain is polarization dependent there is an uncertainty associated with using the average. This uncertainty is calculated to be $\Delta G/G$~0.1%.

3.4. NMR and Q-meter

The Q-meter uses the NMR coil as a sensing probe. This probe couples inductively with the magnetic moments of the nuclei in the material leading to a linear relation between the coil impedance and the complex magnetic susceptibility of the target material. The dispersion near resonance changes sign and has largest values near the Larmor frequency. The absorption, imaginary part, describes the spectral distribution of the precession frequencies of the spins near the NMR Larmor frequency and its integral is proportional to the nuclear polarization.

The Q-meter can be used outside experimental conditions to achieve relative polarization that can be measured to an accuracy of better than 1%. During an experiment, calibration, environmental changes, NMR sampling non-uniformity and inhomogeneous radiation damage to the material can all play an important role in adding uncertainties.

Changes in Q-meter output voltage as a function of holding field have been measured to be smaller than 4.3×10^{-4} over a range of 0–5 T. Under ideal experimental operating conditions of the cryostat the Q-meter circuit tune does not shift and only small changes, $\Delta V/V<1\times10^{-4}$, in the offset of the Q-meter output voltage are seen with respect to the NMR coil coaxial cable temperature.

There are known non-linearities in the Q-meter seen by measuring the power dissipated in the LCR circuit that can arise from changes in the ambient temperature of the Q-meter. The modulator output signal has a small temperature dependence that can be seen with constant input voltage and phase difference. This dependence was studied by measuring the Q-meter output voltage (or absolute polarization) in response to changes of the Q-meter circuit temperature. The relative deviation can change with respect to input signal, but not to a large degree. Several tests were performed at UVA to quantify this deviation. An example using polarized ammonia is shown in Fig. 7. The sample was polarized to 95.05% holding the Q-meter at 21.5 °C. The temperature of the Q-meter was then varied to obtain a trend in polarization with respect to temperature of the Q-meter circuit. The temperature of the Q-meter was measured with an external thermistor adhered to a gold plated copper enclosure around the

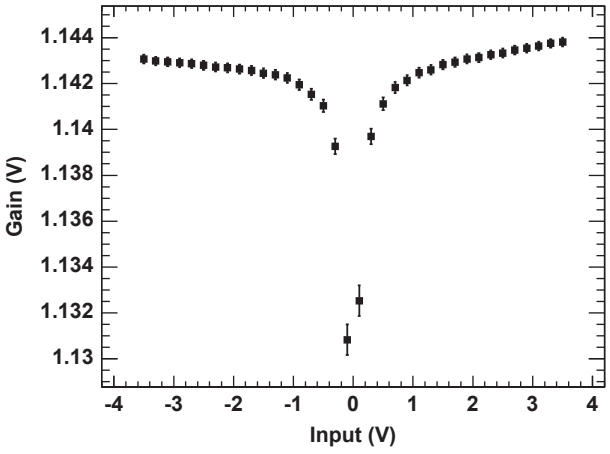

Fig. 6. Yale card gains as a function of input voltage. The normal operating range of the output voltage of the Liverpool Q-meter is ~3 V.

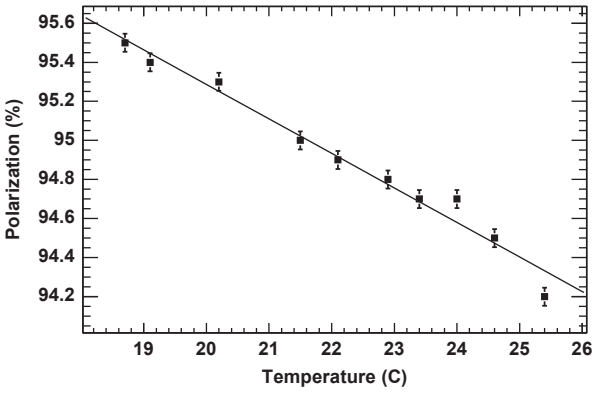

Fig. 7. Polarization dependence on Q-meter temperature using ammonia polarized to 95.05% with Q-meter circuit held at 21.5 °C.

Q-meter circuit. Tests were done on both of the Q-meters used in experiment E08-007. No changes are made in the polarized target analysis from these results but the uncertainty is considered. The experimental data indicated an average temperature of 21.2 ± 1.2 °C, which at a polarization of 95% using a range of 2.4 °C results in an uncertainty less than 0.54%. However, the uncertainty changes slightly depending on the polarization or output voltage of the Q-meter.

The estimated uncertainty in polarization from the Q-meter temperature dependence and NMR circuit issues mentioned is $\Delta P/P$~0.75%, which is an estimation based on the effects seen over the course of the experiment. With continuous data on the Q-meter temperature a small correction can be made to the polarization as a function of temperature. For experiment E08-007 there were only a few temperature readings obtained so only an uncertainty is achievable.

3.5. NMR signal fitting and integration

The TE measurements were carried out after thermalizing during the experiment, without beam and without microwaves. A baseline spectrum was taken by adjusting the magnetic field to be off-resonance. During the TE measurement, data is collected using the NMR baseline with the TE signal spectrum. To compensate for drifts, the first and last 50 channels of the TE spectrum were used for a second degree polynomial fit to the background which was then subtracted to give the final TE spectrum. The final TE spectrum is then integrated. Each of these preceding steps can contribute uncertainty to the final TE area. The signal is of an unknown line shape and so it is integrated using a Riemann sum to obtain the signal area. An error estimate is achieved by combining the variance from the polynomial background fit and the error in the Riemann sum. A TE signal on top of a standard baseline is shown in Fig. 8.

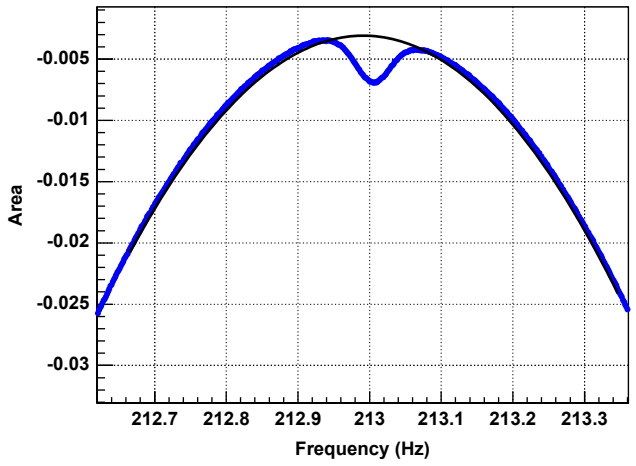

Fig. 8. The TE signal with a polynomial background fit to the baseline.

Enhanced signals were large enough that the uncertainty from the fit and Riemann sum became negligible ($\delta A_E/A_E \ll 0.1\%$). In order to obtain an estimate in the TE Riemann sum, a Gaussian signal of average TE amplitude was generated on a standard baseline and the Riemann sum with background fit was used to obtain an area. It was found that the uncertainty is very much correlated with the slope of the polynomial fit where the signal sits. Accurate baseline and polynomial fit are critical for TE measurements. Depending on the shape of the background the uncertainty in the TE area can be as much as 2%. For the TE measurements in experiment E08-007 the uncertainty in TE area from the Riemann sum $\delta A_{TE}/A_{TE}$ is smaller than or equal to 1.61%.

During the polarized target data analysis, the polynomial fit is checked to ensure a realistic background in relation to the signal location and to minimize fit errors using χ^2-minimization. After the quality of the baselines is checked and the fit errors are minimized the area of the TE and enhanced signals is calculated. In most cases, a quality baseline is ascertained using the one closest to the TE measurement applied for that section of data. If the NMR tune is adjusted or fluctuates due to environmental conditions, the change will not be represented in a baseline taken earlier. Normally 3000 sweeps were used when taking a baseline as to reduce statistical uncertainty. During TE data taking the number of sweeps is kept at 2000 or more to minimize the noise to signal. The uncertainty from the background fit $\Delta A_{fit}/A_{fit}$ is calculated as the percent change in area using the various parameterizations of the polynomial during the χ^2-minimization. The χ^2-minimization requires at least two steps of iteration resulting in at least two sets of polynomial parameters. The extremal set of parameters is used to find the variation in area due to the fit. For experiment E08-007 this value is smaller than or equal to 0.75%. Fig. 9 shows the TE and enhanced signal after baseline and background subtraction.

4. Integrated polarization uncertainties

The total uncertainty from the calibration constant contains error from the TE area (see Section 3.5) as well as error from the TE

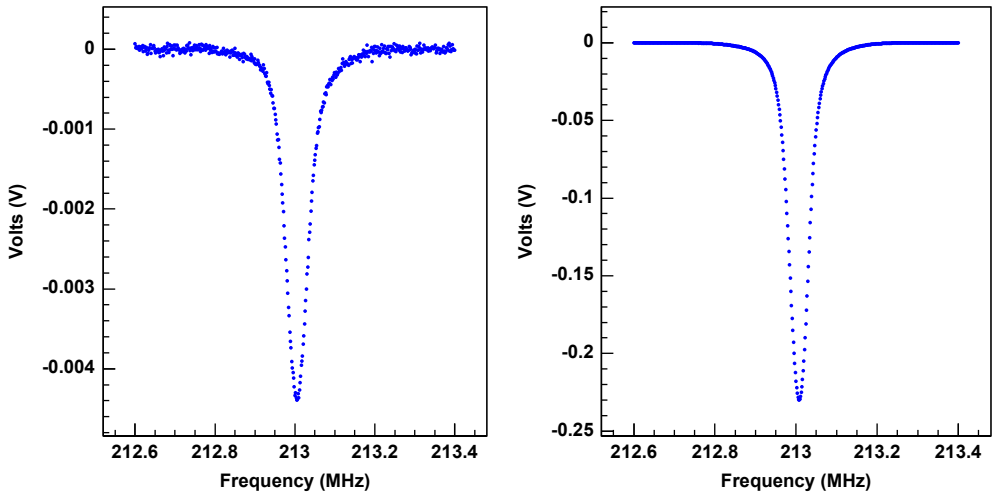

Fig. 9. The TE and enhanced signals after baseline and background subtraction.

polarization. Each separate component is propagated in accordance with Eq. (3). These uncertainties must be combined with the system's instrumental and systematic components. The latter is regulated through a TE fitting algorithm.

4.1. Thermal equilibrium polarization

For TE signals of protons, it is important to reduce the quality factor Q of the NMR circuit to minimize the modulation and the non-linearities. The temperature during the TE was necessarily very regular and only exhibits thermal fluctuations, ~1.52% in area at 1.5 K. Thermalization can take several hours depending on the material's previous polarization state. The most accurate temperature of the material was measured with a liquid helium vapor pressure sensor connected to a Baratron 690A manometer. The standard accuracy of the manometer is about 0.12% with a 10^{-6} full scale resolution. The relation used to convert ^{4}He liquid helium vapor pressure p in Pascal to temperature in Kelvin is [15]

$$T = \sum_{i=0}^{9} a_i \left(\frac{\ln p - b}{c}\right)^i \tag{5}$$

where the constants a_i, b, and c are a set of parameters which depend on the state and temperature scale of the helium. A ^{3}He bulb and manometer were used to check the temperature results. There was very good agreement between the ^{4}He and ^{3}He temperatures, which on average were equivalent within ± 13 mK with helium covering the bulb during the calibration runs. The position of the ^{3}He bulb was ~3 cm above the top cup, while the ^{4}He probe sat more than 5 cm above the full ^{4}He liquid level. The temperature difference maybe due to the distance or calibration variation between the two probes. The difference in the probes, ΔT, is used as the uncertainty in the temperature of the target material and used to calculate the uncertainty in polarization, ~1.45%, during the TE measurements. The uncertainty from ΔT is accounted for in the next section.

The uncertainty in using the ^{4}He vapor pressure probe and manometer is $\Delta p/p$~0.53% which is purely from instrumental precision. This instrumental uncertainty is combined with the error estimate for each pressure reading. The uncertainty in temperature as a function of pressure is expressed as

$$\delta T = \sum_{i=1}^{8} a_i \left(\frac{\ln p - b}{c}\right)^i \frac{\delta p}{pc}. \tag{6}$$

In addition to pressure, the magnetic field strength is required to calculate the TE polarization. The instrumental uncertainty in the magnetic field strength is 0.01%. This value represents the setability of the superconducting magnet power supply. In addition there is an uncertainty associated with the field strength through the target material. Assuming homogeneity in material the LCR circuit is tuned to the Larmor frequency of the proton, 213 MHz, in a 5 T field. Centering the Q-curve by changing the power supply current accurately locates the magnetic field setting to within a defined error. The total estimate of the uncertainty including setability is δB~0.022%. Though quite small, this error is used in the full error propagation of the TE polarization for completeness. Each component of statistical and fit uncertainty as well as the measurements instrumental uncertainty are added together. The final value of TE polarization uncertainty is calculated using the following expression:

$$\delta P_{TE} = \frac{\mu B}{KT}\sqrt{\left(\frac{\delta B}{B}\right)^2 + \left(\frac{\delta T}{T}\right)^2}\,\mathrm{sech}^2\left(\frac{\mu B}{KT}\right). \tag{7}$$

The total uncertainty is established after the fit over a set of measured pressures and areas, see Section 4.3. Because these measurement instrumental uncertainties, δp and δB, are part of the integrated TE polarization uncertainty, δP_{TE}, they are not used as part of the cumulative signal uncertainties listed in the next section.

4.2. Cumulative signal uncertainties

It is necessary to consider all instrumental uncertainties that affect the quality of the polarization. In general, the NMR Q-circuit is susceptible to changes over time such as changes in coil material coupling, coil orientation, vibration, and nuclear chemical changes in material as a function of dose. All of these types of contributions are expected to be negligible and could only be seen over multiple TE measurements. As mentioned the major contributions to the uncertainty in the evaluation of the calibration constant is the uncertainty in the TE signal area and in the temperature of the material while taking the TE measurement. The determination of the TE signal area has errors associated with it from the Riemann sum ΔA_{TE} and the background fit ΔA_{fit}. Another component of polarization uncertainty is the non-linearities of the Q-meter circuit and changes in the electronic length of the $\lambda/2$-cable as a function of temperature of the circuit itself denoted as ΔV_Q. Additional sources of uncertainty come from tuning changes due to magnetoresistance of the coils and cables inside the cryostat, R_B. It is worth noting that using a cold NMR can greatly reduce the uncertainty associated with the NMR tune, see Ref. [16].

Also considered are the shifts in NMR tune during data taking, the uncertainty in the gain voltage ΔV_{Yale}, and the effect of the magnetic field drift in persistent mode during an experimental run ΔB_{drift}. The uncertainty value from the shifts in the NMR tune is a result of averaged effects on polarization seen when the NMR Q-curve changed in time. The magnetic field drifts are taken into account because these changes in field deviate from the field used during the TE measurement resulting in polarization uncertainty.

The uncertainties acquired during the thermal equilibrium that are based on area (A_{TE}), measurement limitations (S_{TE}), the uncertainty estimates due to the systematic effects in the enhanced signal over time (S_E), and gain (G) are all listed in Table 1. The uncertainty associated with averaging the polarization over each run, $\Delta\overline{P}_{run}$, is not strictly expressed in Eq. (4) but is an important contributor and is discussed later in Section 6.

The total uncertainty found in polarization is 2.60%. This uncertainty is prior to the systematics involved in using the data to find the optimal calibration constant as well as the optimization through the use of multiple TE measurements for the same consecutive usage of target material. The value for $\Delta P/P$ from Table 1 contains all errors from Eq. (4) not including $\delta P_{TE}/P_{TE}$ defined in Eq. (7).

Table 1
The relative uncertainties acquired during the thermal equilibrium that are based on area (A_{TE}) and measurement limitations (S_{TE}). Additionally the relative uncertainty estimates due to the systematic effects in the enhanced signal over time S_E and gain (G) are listed. Also included is an error estimate from charge averaging over each experimental run.

(#)	Type	Source	Error (%)
(1)	S_{TE}	ΔT	1.45
(2)	A_{TE}	ΔA_{TE}	1.61
(3)	A_{TE}	ΔA_{fit}	0.75
(4)	S_E	R_B	0.50
(5)	S_E	ΔV_Q	0.75
(6)	S_E	NMR-tune	0.47
(7)	S_E	ΔB_{drift}	0.25
(8)	G	ΔV_{Yale}	0.10
(9)	–	$\Delta\overline{P}_{run}$	0.50
		$\Delta P/P$	2.60

4.3. TE fitting algorithm

A systematic procedure to extract the most information from the data was established to obtain each calibration constant for a given time period. An algorithm was developed to systematically evaluate the quality of the area and pressure data taken during a TE and determine whether the TE was usable. The algorithm also designates the set of points to be used in the fit to obtain the optimal area with respect to pressure and vice versa.

At thermal equilibrium, the NMR signal area over a region of controlled pressure should exhibit only small thermal fluctuations. To quantify the allowance of thermal fluctuation a limit is set on the deviation in area of 2% at 1.5 K. The limit comes directly from measurements of the maximum point to point spread from fluctuations seen at true thermal equilibrium. The system is only considered at thermal equilibrium with changes in area at this limit or smaller. Both the area and pressure should be flat over the series of points used in the TE measurement. Additional constraints are used to dismiss data that has not had an appropriate relaxation time or not reached equilibrium due to changes in the cryostat. These constraints are defined using a two parameter line fit to study the slope of the line coming in and going out of the flattest range in the localized set of data points in which a TE has been taken. A limit can then be set and used as a safe bound to flag the range of TE points as *usable*. This quantification can then be used to judge the quality of TE data.

4.3.1. TE fitting procedure

The procedure checks over the full range of the TE area and pressure measurements selecting the data with the smallest slope over the largest set of points. The criteria for being usable was a requirement of at least six points in area (pressure) spanning the time range in which a fit to a two parameter line returns a slope less than 0.0035 area/min (Torr/min). The slope limit comes from an allowance of 2% change from point to point in TE area under a one parameter line hypothesis over six points. If this condition was met, the TE was classified as usable. All fits require the same degrees of freedom and same time range in the area and pressure. The starting points are a contiguous collection of six with the smallest slope from the two parameter line fit in the TE data. The number of contiguous points in the final one parameter line fit is increased until the two parameter line fit slope condition was no longer met or the uncertainty in the one parameter line fit increases with the addition rather than decreases. The TE data points in the time sequence are increased one at a time, alternating from before the flat most region to after, under the given constraints. The one parameter line fit is then used to obtain the final area and pressure and associated uncertainties in these values. Fit examples of both the one and two parameter line fits are shown in Fig. 10. The error bar associated with each point in the fit is the standard error from multiple sweeps resulting in a statistical uncertainty associated with the N number of sweeps ($1/\sqrt{N}$ relative) combined with the instrumental uncertainties discussed in Section 3.5 for area and Section 4.1 for pressure. The fit results from pressure are transformed to temperature to find the P_{TE}. The uncertainty from pressure line fit is used in Eq. (6) to find the uncertainty in temperature which is then used in Eq. (7) to acquire the uncertainty in δP_{TE}. The area and uncertainty from the line fit are then used to obtain the final calibration constant and associated uncertainty.

In the procedure described, the same maximal slope limit is used in both pressure and area, which is reasonable at thermal equilibrium. Area and pressure can both approach thermal equilibrium from vastly different trends depending on the initial conditions and state of the cryostat. An alternative usability criterion that is more sensitive to separate changes in area and pressure would be to use a limit based on relative percentage of the quantities in the fit. Using 0.2% of the one parameter line fit result leads to the same TE usability set as the mentioned fix slope

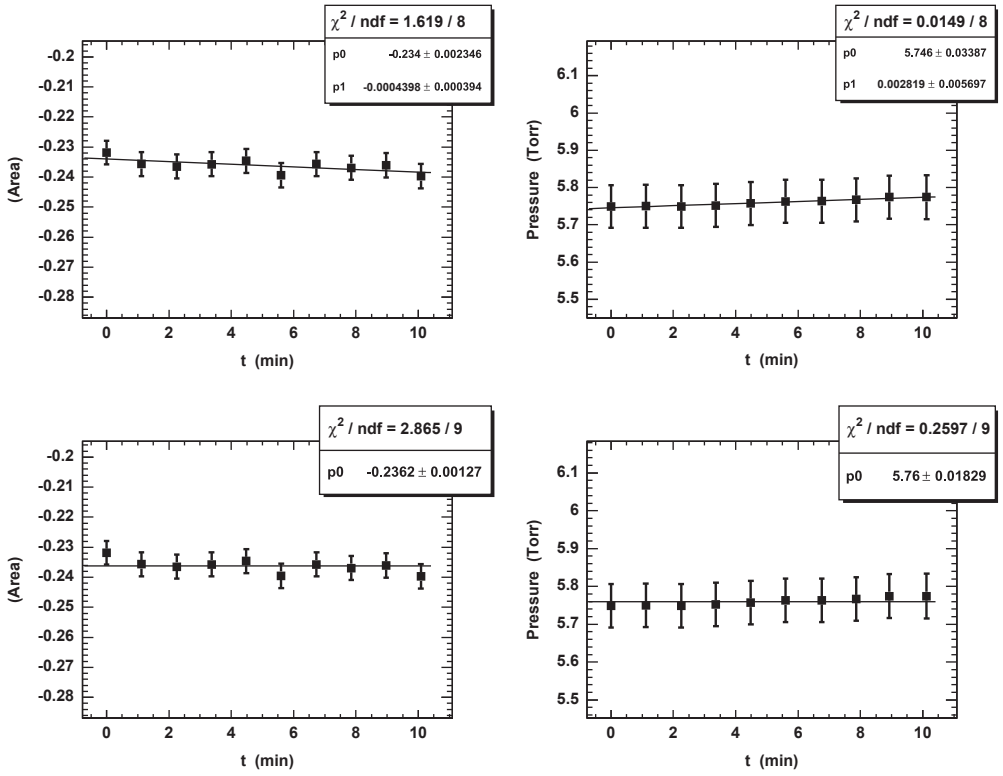

Fig. 10. Example of fits in area and pressure analysis for TE. The top left (right) shows the two parameter check on the slope of the line for area (pressure). The bottom left (right) shows the final one parameter fit to a one parameter line for area (pressure).

limit. However, this method proves to be much more useful in testing the changes in area and pressure slightly before or after actual thermal equilibrium.

4.3.2. Uncertainty in procedure

The value in the one parameter line fit results in the final fit is compared to the fit using only the initial six points. This variation is used as a systematic uncertainty in the procedure. If the initial six points are the only points that pass all constraints for that TE then the largest residual in the fit is used as the systematic uncertainty. A systematic uncertainty is found for each area and pressure fit. This systematic component reflects the quality of the TE data for area and pressure within procedural constraints over the final range of points separate from the fit and statistical components. The error is added to the resulting error for each fit to obtain δT used in Eq. (7) and the error in area δA_{TE} used to find the error in Eq. (4).

Finally, if there are multiple TE measurements taken over the same consecutive usage of material, the set of calibration constants are used in a one parameter line fit. Each TE must pass the criteria for being usable. The final fit was performed using a χ^2-minimization weighting each calibration in the fit by its combined total uncertainty. The minimized uncertainty from the fit was then used as the final error for that calibration constant. These details are outlined in the next section.

5. Calibration uncertainty minimization

The cumulative uncertainty in the calibration constant consists of the combined error of all terms in Eq. (4) with subscript *TE*. The calibration constants and uncertainties for experiment E08-007 are shown in Fig. 11. The *x*-axis indicates the sequence order in which the measurement was taken in the experiment. Calibration measurements taken on consecutively used material are indicated at the half-way points in the sequence. The open points indicate the calibration constants for the top cup and the other are for the bottom cup. All calibration constants are negative so the absolute value is shown. During experiment E08-007 there was no time to acquire any more than two TE calibrations for each consecutively used material after which the material was removed from the cup for experimental configuration changes. Most often one of the two TE calibrations was of poor quality not passing the *usable* criteria. This was due to the calibration data being taken prior to true

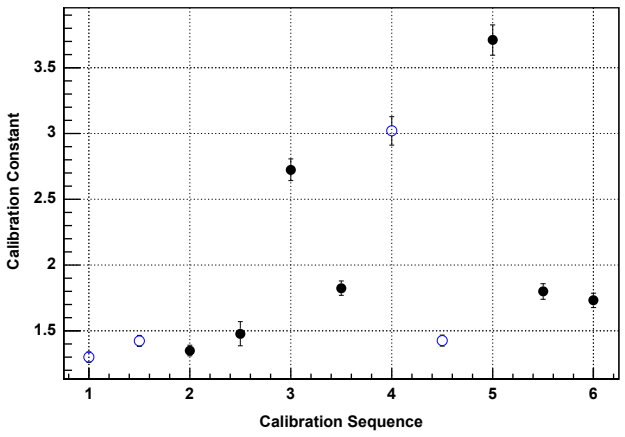

Fig. 11. All calibration constants for experiment E08-007 with the cumulative TE uncertainty. The *x*-axis indicates that the sequence order the measurement was taken in the experiment. Calibration measurements taken on consecutively used material are indicated at the half-way points in the sequence. The open data points represent the top cup data and the closed data points represent data for the bottom cup. All calibration constants are negative so the absolute value is plotted.

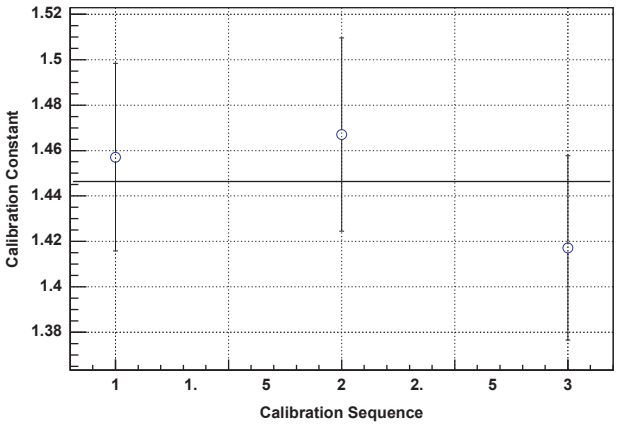

Fig. 12. Calibration constants with 3% error taken during the experiment commissioning phase with ammonia that had not been disturbed. This results in an uncertainty of 2.4% after a linear fit. All calibration constants are negative so the absolute value is plotted.

thermal equilibrium. It is not expected that all values of the calibration constants should be the same being that every time the material is removed and put back into the cell a new material coupling is made to the NMR loop. Radiation damage and annealing as well as material packing and slight changes to the NMR loop orientation with respect to the magnet field can all lead to shifts in the calibration constant. What is expected is that the calibration constant stays the same for material not yet removed from the target insert. If multiple high quality calibration measurements are taken on consecutively used undisturbed ammonia then all values of the calibration constant should be the same within the error bars defined by the contributions to Eq. (4) with subscript *TE*. In this case, multiple TE measurements can reduce the overall uncertainty by using a linear hypothesis encompassing more information to obtain an optimal calibration constant. Fig. 12 shows an example of calibration constants from TE measurements taken during the experiment commissioning. The ammonia had not been disturbed and three high quality TE measurements had been performed several days apart. In this example each measurement resulted in an uncertainty around 3%, after the linear fit the uncertainty was reduced to 2.4%.

It is also possible that the TE measurement was not good according to the algorithm's criteria or that a larger systematic change has occurred. Such changes include displacement of the NMR coil, large shifts in target material (target coil coupling changes), or large NMR tune changes which are all possible over the course of an experiment. If determined that such an effect has occurred and can be seen in the resulting calibration constant then the uncertainty must include the new systematic effect over that set of runs. That systematic effect would be determined by the residual of the calibration constants for that set of data. Fortunately there is no indication of this in the E08-007 data. Greater reduction in uncertainty is always possible with additional quality TE measurements that can go into the final fit of the calibration constants. The results of this minimization are discussed for experiment E08-007 in the next section.

5.1. Final calibration errors

Table 2 shows a summary of the calibration constants and corresponding uncertainties for experiment E08-007. For all production data a 5.0 T field oriented at 6° off the beam axis was used. The Cup column indicates the results for the top (T) or bottom (B) target cups if both were used during the experiment. Some of the TE measurements were not used due to poor quality TE

Table 2
The date in which the target material was installed and then removed is listed along with the electron beam energy, label for top (T) or bottom (B) cup, the final calculated calibration constant, whether the TE was flagged as usable or not, and finally the TE start time from the experimental record used to find the TE data.

Date	E_{Beam} (GeV)	Cup	C_{TE}	Usable	TE start
3/10–3/12	2.2	T	−1.299 (3.05%)	Yes	3–10 16:21:50
			−1.422 (2.97%)	No	3–12 16:42:00
3/10–3/12	2.2	B	−1.349 (3.06%)	Yes	3–10 16:56:55
			−1.477 (6.20%)	Yes	3–12 17:30:20
4/17–4/19	1.7	B	−2.724 (3.02%)	No	4–17 09:08:20
			−1.823 (3.01%)	Yes	4–17 17:36:05
4/17–4/19	1.7	T	−3.020 (3.58%)	No	4–26 13:10:00
			−1.424 (2.94%)	Yes	4–30 01:30:25
4/30–5/5	1.1	B	−3.711 (3.12%)	No	4–26 13:40:25
			−1.799 (3.28%)	Yes	4–30 03:00:35
4/30–5/5	1.1	B	−1.731 (3.18%)	Yes	5–2 20:30:00

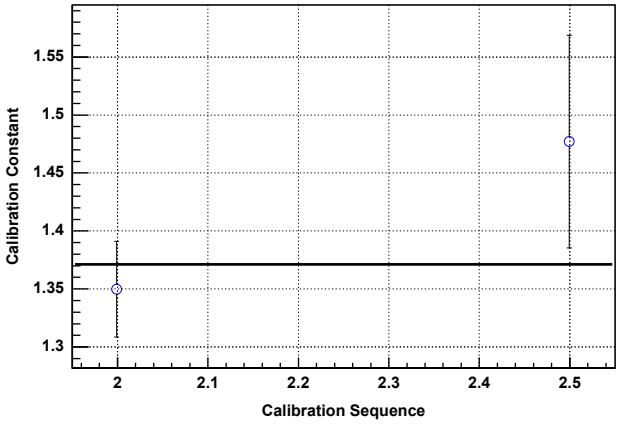

Fig. 13. Calibration constants from E08-007 taken with ammonia that had not been disturbed. This results in an uncertainty of 3.76% after a linear fit.

conditions. The TE measurements were flagged according to the algorithms criteria indicated in the Usable column. Also listed is the TE start time which was used to locate the TE in the polarization data. For configurations with multiple TE data, a final fit is used to produce the result used. As mentioned the final step of uncertainty minimization is to use a linear hypothesis to fit the set of calibration constants from multiple TE measurements on consecutively used material. This step is an essential part of the uncertainty minimization associated with the TE measurements but is only possible when there have been no changes to the calibration constant within error bars and all TE measurements pass the quality constraints in the algorithm. This implies that there have been negligible changes to the NMR coil material coupling from measurement to measurement. Naturally, a greater error reduction can be made using more TE measurements. From Table 2 one can see that there is only one set of TE measurements where both have been flagged as good. The final fit using −1.477 (6.20%) and −1.349 (3.06%) leads to a calibration constant of −1.371 (3.76%). The plot in Fig. 13 shows the two calibration constants and linear fit. Because the error from the TE measurement was quite large for one of the points the uncertainty minimization is not to the degree as previously seen in Fig. 12.

A summary of calibration constants and uncertainties over the sets of E08-007 runs are listed in Table 3. The Hall A configuration consisted of two detector arms collecting data simultaneously. Both right and left arm data acquisition runs are listed along with the appropriate cup used for that set of runs.

Table 3
The relative uncertainty over applied experimental run range with respect to the data taken on the left or right arm, with the top or bottom cups over the all runs for experiment E08-007.

Run Range	Arm	Cup	C_{TE}
3061–3070	Left	T	−1.299 (3.05%)
3071–3084	Left	B	−1.371 (3.76%)
3085–3130	Left	T	−1.299 (3.05%)
4599–4695	Left	B	−1.823 (3.01%)
5339–5344	Left	T	−1.424 (2.87%)
5345–5346	Left	B	−1.799 (3.28%)
5347–5484	Left	B	−1.731 (3.18%)
22146–22155	Right	T	−1.299 (3.05%)
22156–22172	Right	B	−1.371 (3.76%)
22173–22217	Right	T	−1.299 (3.05%)
23540–23618	Right	B	−1.823 (3.01%)
24113–24118	Right	T	−1.424 (2.87%)
24120–24121	Right	B	−1.799 (3.28%)
24122–24258	Right	B	−1.731 (3.18%)

6. Polarization data

Once the calibration constant is obtained along with the enhanced NMR signal integration, the Yale card gains and uncertainties, it is possible to calculate the final polarization which can be used in experimental analysis.

6.1. Charge averaging

Each target event is stamped with time but to be useful each target event must be associated with a particular data acquisition run which recorded the physics data. All the events written to the target data files are broken down and configured into runs based on the run start and stop time. The polarizations measured over time are charge averaged using the dose on the target material, see Fig. 2. The BCM currents are averaged over time between target events leading to a dose which can be associated with a polarization for a given duration. The BCM currents are then used to calculate the dose on the target material for that run and charge average the polarizations. The method of weighting each polarization measurement with charge in the average eliminates uncertainty associated with jumps in polarization due to beam trips. The charge averaged polarization for a single run is given by

$$\overline{P}_{run} = \sum_{i}^{n} Q_i P_i \tag{8}$$

where P_i is the ith polarization measurement in the total n for that run. The weight Q_i is the beam dose averaged from target event $i-1$ to i and normalized to the total dose the target received for that run. The charge averaged polarization for each run is what is required for the physics analysis of the scattering asymmetry which is also calculated for each run.

The uncertainty in the charge weighted average of polarization must also be calculated for each run. The error estimate for the charge averaged polarization in Eq. (8) is defined as

$$\Delta\overline{P}_{run} = \sqrt{\sum_{i}^{n} Q_i^2 (\overline{P}_{run} - P_i)^2}. \tag{9}$$

The quantity $\Delta\overline{P}_{run}$ represents the dispersion from the weighted average of the uncorrelated polarization measurements over a single run. The use of the average implies that the polarization data follows a linear trend over the course of a run. This neglects the true exponential line shape of the polarization decay with beam dose. The uncertainty $\Delta\overline{P}_{run}$ encompasses the error in using a linear approximation as well as polarization fluctuations due to cryogenic changes or manual adjustments due to the microwave

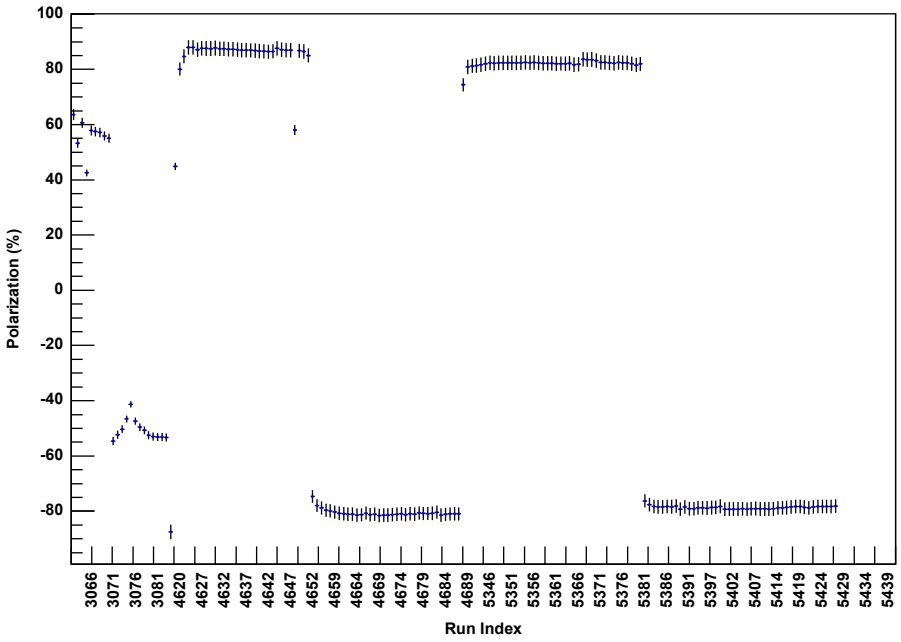

Fig. 14. The final charge averaged polarization and uncertainty per run.

frequency. For a steady production run without adjustments to the microwave frequency in experiment E08-007 the uncertainty in the weighted average is $\Delta\overline{P}_{run}/\overline{P}_{run} < 0.1\%$. But the aforementioned changes can lead to sudden drops or increases in polarization increasing the uncertainty in the average. A quality constraint is imposed at 0.5% which is on the level of moderate adjustments to the microwave frequency. Any run with a $\Delta\overline{P}_{run}/\overline{P}_{run} > 0.5\%$ is excluded from the physics analysis.

6.2. Polarization results

The final polarization and uncertainty per run is shown in Fig. 14. The largest of these uncertainties is 3.90% relative.

7. Conclusion and further reduction

The uncertainties introduced by TE area ΔA_{TE}, background fit ΔA_{fit}, Q-meter ΔQ_T, Yale card ΔV_{Yale}, magnetic field variation ΔB_{drift}, and variation in polarization over a run ΔP_{run} all have additional dependence that makes the uncertainty change over the course of the experiment. Some of the dependence are simply changing conditions in the experiment and some change as a function of polarization. In the present results the uncertainty in ΔA_{TE} and ΔA_{fit} is estimated based on extremal conditions throughout the entire experiment. This is done to avoid underestimating an essential component of error. The values used for ΔT, ΔV_Q, and R_B are estimates based on averages over the experiment. The value used in ΔT is based on a median temperature difference seen in the ^{4}He vapor pressure and ^{3}He bulb during TE measurements. The average difference is consistent over the set of TE measurements. The error ΔP_{run} was calculated for each production run and a maximum of 0.5% is used as the expected limit from changes due to microwave pumping adjustments and polarization decay. The value ΔP_{run} can be much higher for runs started while the target was still polarizing or non-optimum microwave adjustments. Further uncertainty reduction for certain runs can be made by implementing a run dependence to each of the listed components of uncertainty. Because these uncertainties are small an additional run dependence will not have a large effect.

For future experiments there are several key points that can be used to keep the acquired error to a minimum. It is possible to reduce the uncertainties introduced by TE area ΔA_{TE}, and background fit ΔA_{fit} by making sure that the TE peak is centered with a good baseline taken with at least three thousand sweeps. If the Q-meter temperature is regulated with a chiller, the deviation in temperature is reduced as is ΔQ_T. It is also important to have Q_T as part of the data stream so a simple correction to the polarization can be made as a function of Q-meter temperature. Checking the position of the NMR signal frequently can reduce the effects of the uncertainty in magnetic field variation ΔB_{drift}. The only reason why ΔB_{drift} has a non-zero value for experiment E08-007 was a malfunction in the quench protector in the power supply. Checking the stability of the NMR signal during Hall access and after the NMR tune can reduce unexpected changes once the experimental Hall goes to beam permit.

The largest reduction of uncertainty comes from having multiple TE measurements over the same consecutive use of a target material and using a χ^2-minimization with a one parameter line hypothesis to fit the multiple calibration constants. The more quality TE measurements that are taken the more the uncertainty can be reduced. Many TE measurements in the present study did not pass the constraints in the algorithm. This implies that the measurements were taken when the system did not fully reach thermal equilibrium or that enough points were not recorded once thermal equilibrium was reached.

During experiments, time for TE measurements can frequently be limited. Obtaining multiple quality TE measurements can help to significantly reduce uncertainty using the procedure outlined here, however multiple TE measurements that cannot pass the quality constraints are not useful. For the sake of polarization uncertainty reduction it is critical to prioritize blocks of time specifically for waiting for true thermal equilibrium for multiple TE measurements.

Acknowledgments

The author thanks D. Crabb, D. Day, O. Rondon, the Jefferson Lab target group, as well as the staff of the Thomas Jefferson National Accelerator Facility who made this research possible. This work was supported by DOE contract DE-FG02-96ER40950.

References

[1] M. Jones, et al., Physical Review Letters 84 (2000) 1398.
[2] O. Gayou, et al., Physical Review Letters 88 (2002) 092301.
[3] I. Qattan, et al., Physical Review Letters 94 (2005) 142301.
[4] D.G. Crabb, D.B. Day, Nuclear Instruments and Methods in Physics Research Section A 356 (1995) 9.
[5] K.H. Althoff, et al., in: W. Meyer (Ed.), Proceedings of the 4th Workshop on Polarized Target Materials and Techniques, University of Bonn, Bonn, 1984, p. 23.
[6] D.G. Crabb, in: W. Meyer, E. Steffens, W. Thiel (Eds.), Proceedings of the 9th International Symposium on High-Energy Spin Physics, vol. 2, Springer Verlag, Germany, 1991, p. 289.
[7] S. Brown, et al., in: W. Meyer (Ed.), Proceedings of the 4th Workshop on Polarized Target Materials and Techniques, University of Bonn, Bonn, 1984, p. 66.
[8] T.O. Niinikoski, J.M. Rieubland, Physics Letters 72A (1979) 141.
[9] D.A. Hill, J.J Hill, Argonne National Laboratory Report, ANL-HEP-PR-81-05, 1981.
[10] L.G. DeMarco, A.S. Brill, D.G. Crabb, Journal of Chemical Physics 108 (1998) 1423.
[11] J.C. Denard, A. Saha, High Accuracy Beam Current Monitor System For CEBAF Experimental Hall A, Jefferson Lab Note: ACT01-12, 2001.
[12] G.R. Court, et al., Nuclear Instruments and Methods in Physics Research Section A 324 (1993) 433.
[13] D. Crabb, W. Meyer, Annual Review of Nuclear and Particle Science 47 (1997) 67.
[14] O. Kahn, Molecular Magnetism, VCH, New York, 1993.
[15] R.J. Donnelly, C.F. Barenghi, Journal of Physical and Chemical Reference Data 27 (1998) 1217.
[16] G.R. Court, et al., Nuclear Instruments and Methods in Physics Research Section A 527 (2004) 253.